The Astrophysical Journal, 632:1093–1098, 2005 October 20

HADRONIC HIGH-ENERGY GAMMA-RAY EMISSION FROM THE MICROQUASAR LS I +61 303

Gustavo E. Romero[1]
Instituto Argentino de Radioastronomía (IAR), Casilla de Correo 5, 1894 Villa Elisa, Argentina; romero@irma.iar.unlp.edu.ar

Hugo R. Christiansen
State University of Ceara, Physics Department, Avenida Paranjana 1700, 60740-000 Fortaleza-CE, Brazil; hugo@uece.br

and

Mariana Orellana[2]
Instituto Argentino de Radioastronomía (IAR), Casilla de Correo 5, 1894 Villa Elisa, Argentina; morellana@irma.iar.unlp.edu.ar
Received 2005 March 28; accepted 2005 June 28

ABSTRACT

We present a hadronic model for gamma-ray production in the microquasar LS I +61 303. The system is formed by a neutron star that accretes matter from the dense and slow equatorial wind of the Be primary star. We calculate the gamma-ray emission originating from *pp* interactions between relativistic protons in the jet and cold protons from the wind. After taking into account opacity effects on the gamma rays introduced by the different photon fields, we present high-energy spectral predictions that can be tested with the new-generation Cerenkov telescope MAGIC.

Subject headings: gamma rays: observations — gamma rays: theory — stars: individual (LS I +61 303) — X-rays: binaries

Online material: color figures

1. INTRODUCTION

LS I +61 303 is a Be X-ray binary that presents unusually strong and variable radio emission (Gregory & Taylor 1978). The X-ray emission is weaker than in other objects of the same class (e.g., Greiner & Rau 2001) and shows a modulation with the radio period (Paredes et al. 1997). The most recent determination of the orbital parameters (Casares et al. 2005) indicates that the eccentricity of the system is 0.72 ± 0.15 and that the orbital inclination is $\sim 30^\circ \pm 20^\circ$. The best determination of the orbital period ($P = 26.4960 \pm 0.0028$) comes from radio data (Gregory 2002). The primary star is a B0 V star with a dense equatorial wind. Its distance is $\sim$2 kpc. The X-ray/radio outbursts are triggered 2.5–4 days after the periastron passage of the compact object, usually thought to be a neutron star. These outbursts can last until well beyond the apastron passage.

Recently, Massi et al. (2001) detected the existence of relativistic radio jets in LS I +61 303, which makes of it a member of the microquasar class. Microquasars are thought to be potential gamma-ray sources (Paredes et al. 2000; Kaufman Bernadó et al. 2002; Bosch-Ramon et al. 2005a), and, in fact, LS I +61 303 has long been associated with a gamma-ray source, first with the *COS B* source 2CG 135+01 and later on with 3EG J0241+6103 (Gregory & Taylor 1978; Kniffen et al. 1997). The gamma-ray emission is clearly variable (Tavani et al. 1998), and it has recently been shown that the peak of the gamma-ray light curve is consistent with the periastron passage (Massi 2004), contrary to what happens with the radio/X-ray emission, which peaks *after* the passage.

The matter content of microquasars' jets is unknown, although in the case of SS 433 iron X-ray line observations have proved the presence of ions in the jets (Kotani et al. 1994, 1996; Migliari et al. 2002). In the present paper we assume that relativistic protons are part of the content of the observed jets in LS I +61 303, and we develop a simple model for the high-energy gamma-ray production in this system, with specific predictions for Cerenkov telescopes like the Major Atmospheric Gamma Imaging Cerenkov Telescope (MAGIC). We emphasize that our model is not opposed, but rather complementary to pure leptonic models such as those presented by Bosch-Ramon & Paredes (2004) and Bosch-Ramon et al. (2005a), since the leptonic contribution might dominate at lower gamma-ray energies and after the periastron passage. In § 2 we describe the basic features of the model, and then we present the calculations and results.

2. GENERAL PICTURE

A hadronic model for the gamma-ray emission in microquasars with early-type companions has already been developed by Romero et al. (2003). This model, however, is limited to the simple case of a massive star with a spherically symmetric wind and a compact object in a circular orbit. Here we consider a B-type primary with a wind that forms a circumstellar outflowing disk of density $\rho_w(r) = \rho_0(r/R_*)^{-n}$ (Gregory & Neish 2002). The continuity equation implies a wind velocity of the type $v_w = v_0(r/R_*)^{n-2}$. We consider that the wind remains mainly near the equatorial plane, confined in a disk with half-opening angle $\phi = 15^\circ$, with $n = 3.2$, $\rho_0 = 10^{-11}$ g cm^{-3}, and $v_0 = 5$ km s^{-1} (Martí & Paredes 1995).

The modeled properties of the system are expressed in terms of the orbital phase ψ ($\psi = 0.23$ at the periastron passage according to the latest determination by Casares et al. 2005), which is related to the separation between the stars by $r(\psi) = a(1 - e^2)/\{1 - e\cos[2\pi(\psi + 0.73)]\}$, where a is the semimajor axis of the orbit and e is the eccentricity. The wind accretion rate onto the compact object of mass M_c can be estimated as

$$\dot{M}_c = \frac{4\pi(GM_c)^2\rho_w(r)}{v_{\rm rel}^3}, \qquad (1)$$

where $v_{\rm rel}$ is the relative velocity between the neutron star (moving in a Keplerian orbit) and the circumstellar wind, assumed to be flowing radially on the equatorial plane.

[1] Member of CONICET, Argentina.
[2] Fellow of CONICET, Argentina.

Following the basic assumption of the jet-disk symbiosis model (Falcke & Biermann 1995), we assume that the accretion rate is coupled to the kinetic jet power by

$$Q_j = q_j \dot{M}_c c^2, \tag{2}$$

where $q_j \sim 0.1$ is the coupling constant. Most of this power consists of cool protons that are ejected with a macroscopic Lorentz factor $\Gamma \sim 1.25$ (Massi et al. 2001). Only a small fraction $q_j^{\rm rel} \sim 10^{-3}$ is in the form of relativistic hadrons. The relativistic jet is confined by the pressure of the cold particles ($P_{\rm cold} > P_{\rm rel}$), which expand laterally at the local sound speed.

The jet axis, z, is assumed to be normal to the orbital plane. The jet is conical, with a radius $R_j(z) = z(R_0/z_0)$, where z_0 is the injection point and R_0 is the initial radius of the jet. We adopt $z_0 = 10^7$ cm and $R_0 = z_0/10$ as reasonable values (see Romero et al. 2003; Bosch-Ramon et al. 2005a, who deal with similar jets, for additional details). The relativistic proton spectrum is a power law $N'_p(E'_p) = K_p E'^{-\alpha}_p$, valid for $E'^{\rm min}_p \le E'_p \le E'^{\rm max}_p$ (in the jet frame). The corresponding relativistic proton flux is $J'_p(E'_p) = (c/4\pi)N'_p(E'_p)$. Since the jet expands in a conical way, the proton flux evolves with z as

$$J'_p(E'_p) = \frac{c}{4\pi} K_0 \left(\frac{z_0}{z}\right)^2 E'^{-\alpha}_p, \tag{3}$$

where the assumption of the conservation of the number of particles is implicit (see Ghisellini et al. 1985) and a prime refers to the jet frame. Using relativistic invariants, it can be shown that the proton flux, in the lab (observer) frame, becomes (e.g., Purmohammad & Samimi 2001)

$$J_p(E_p,\theta) = \frac{cK_0}{4\pi}\left(\frac{z_0}{z}\right)^2 \times \frac{\Gamma^{-\alpha+1}\left(E_p - \beta_b\sqrt{E_p^2 - m_p^2c^4}\cos\theta\right)^{-\alpha}}{\left[\sin^2\theta + \Gamma^2\left(\cos\theta - \beta_b E_p/\sqrt{E_p^2 - m_p^2c^4}\right)^2\right]^{1/2}}. \tag{4}$$

In this expression, Γ is the jet Lorentz factor, θ is the angle subtended by the proton velocity direction (which is roughly the same as that of the emerging photon) and the jet axis (note that then $\theta \approx \theta_{\rm obs}$), and β_b is the bulk velocity in units of c. We make all calculations in the lab frame, where the cross sections for pp interactions have suitable parametrizations.

The number density n'_0 of particles flowing in the jet at R_0 and the normalization constant K_0 can be determined as in Romero et al. (2003). In the numerical calculations of § 3 we have considered $E'^{\rm max}_p = 100$ TeV, $E'^{\rm min}_p = 1$ GeV, $\Gamma = 1.25$, and $\alpha = 2.2$ (see the list of the assumed parameters in Table 1). The assumed maximum energy is consistent with the jet size and shock acceleration with an efficiency $\sim$0.01–0.1.

The matter from the wind can penetrate the jet from the side, diffusing into it as long as the particle gyroradius is smaller than the radius of the jet. This imposes a constraint on the value of the magnetic field in the jet, $B_{\rm jet} \ge E_k/(eR_0)$, where $E_k = m_p v_{\rm rel}^2/2$. For the periastron passage (E_k maximum), $B_{\rm jet} \ge 2.8 \times 10^{-6}$ G results, which is surely satisfied. However, some effects, such as shock formation on the boundary layers, could prevent some particles from entering into the jet. Given our ignorance of the microphysics involved, we adopt a parameter f_p that takes into account particle rejection from the boundary in a phenomenological way. In a conservative approach, we adopt $f_p \sim 0.1$.

TABLE 1

Basic Parameters Assumed for the Model

Parameter	Symbol	Value
Mass of the compact object	M_c	1.4 $M_\odot$
Jet's injection point	z_0	$50R_g$[a]
Initial radius	R_0	$z_0/10$
Mass of the companion star	M_*	10 $M_\odot$
Radius of the companion star	R_*	10 $R_\odot$
Effective temperature of the star	$T_{\rm eff}$	22,500 K
Density of the wind at the base	ρ_0	10^{-11} g cm^{-3}
Initial wind velocity	v_0	5 km s^{-1}
Jet's Lorentz factor	Γ	1.25
Minimum proton energy	$E'^{\rm min}_p$	1 GeV
Maximum proton energy	$E'^{\rm max}_p$	100 TeV
Penetration factor	f_p	0.1
Eccentricity	e	0.72
Orbital period	P	26.496 days
Index of the jet proton distribution	α	2.2

[a] $R_g = GM_c/c^2$.

Some of the particles entering the jet flow would be immediately accelerated to the jet velocity (by Coulomb interactions or wave-particle interactions). As a consequence, the jet should be slowed down during its motion through the equatorial wind. However, it is a fact that the jet survives this interaction, since it is seen at radio wavelengths far beyond the wind region, up to distances of $\sim$400 AU (Massi et al. 2001, 2004). Since the bulk velocity seems not to be very high (Massi et al. 2001), and hence its change does not affect seriously the calculations of the gamma-ray emissivity, we neglect, in what follows, the effects of a macroscopic deceleration. The reader interested in the case of the hadronic gamma-ray emission of a jet slowed down to rest by the effects of the wind and the resulting standing shock wave as the major source of radiation is referred to the recent treatment presented by Romero & Orellana (2005).

In Figure 1 we show a sketch of the general situation, and in Figure 2 we show the orbit of the system and the corresponding phases.

3. GAMMA-RAY EMISSION

Relativistic protons in the jet interact with target protons in the wind through the reaction channel $p + p \rightarrow p + p + \xi_{\pi^0}\pi^0 + \xi_{\pi^\pm}(\pi^+ + \pi^-)$, where ξ_π is the corresponding multiplicity. Then pion decay chains lead to gamma-ray and neutrino emission. The differential gamma-ray emissivity from π^0 decays can be expressed as (e.g., Aharonian & Atoyan 1996)

$$q_\gamma(E_\gamma,\theta) = 4\pi\sigma_{pp}(E_p)\frac{2Z^{(\alpha)}_{p\rightarrow\pi^0}}{\alpha} J_p(E_\gamma,\theta)\eta_A, \tag{5}$$

where $Z^{(\alpha)}_{p\rightarrow\pi^0}$ is the so-called spectrum-weighted moment of the inclusive cross section (see, for instance, Gaisser 1990) and $J_p(E_\gamma)$ is the proton flux distribution (eq. [4]) evaluated at $E = E_\gamma$. The cross section $\sigma_{pp}(E_p)$ for inelastic pp interactions at energy $E_p \approx 6\xi_{\pi^0}E_\gamma/K$, where $K \sim 0.5$ is the inelasticity coefficient and $\xi_{\pi^0} = 1.1(E_p/{\rm GeV})^{1/4}$, can be represented for $E_p \ge 1$ GeV by

$$\sigma_{pp}(E_p) \approx 30[0.95 + 0.06\log(E_p/{\rm GeV})] \text{ mbarn}.$$

Finally, the parameter η_A takes into account the contribution from different nuclei in the wind and in the jet (for the standard composition of cosmic rays and interstellar medium, $\eta_A \sim 1.4$).

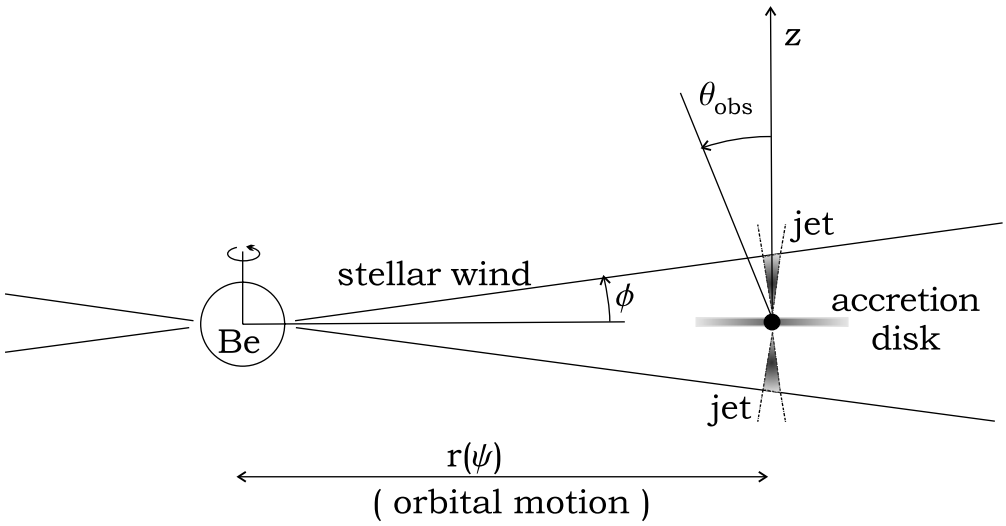

FIG. 1.—Sketch of the situation described in this paper (not drawn to scale).

The spectral energy distribution is

$$L_\gamma(E_\gamma,\theta) = E_\gamma^2 \int_V n(\boldsymbol{r}')\, q_\gamma(E_\gamma,\theta)\, d^3\boldsymbol{r}', \tag{6}$$

where V is the interaction volume between the jet and the circumstellar disk. The particle density of the wind that penetrates the jet is $n(r) \approx f_p \rho_w(r)/m_p$.

In our calculations, we adopt a viewing angle of $\theta = 30^\circ$ in accordance with the average value given by Casares et al. (2005). In Figure 3 we show a three-dimensional plot that shows the evolution of the gamma-ray spectral energy distribution as a function of the orbital phase. The other two plots in this figure show cuts at both the periastron and apastron and the luminosity evolution with the orbital phase at 100 GeV. In both cases we show the unabsorbed (*dashed lines*) and the absorbed (*solid lines*) curves. This absorption is discussed in § 4.

At the periastron passage the unattenuated luminosity is $\sim 10^{33}$ ergs s^{-1}. We can make a simple order-of-magnitude estimate of this value. The accretion rate at the periastron is $\sim 3 \times 10^{17}$ g s^{-1}. This means that the total power in relativistic protons should be $Q_j^{\rm rel} = 10^{-3}\dot{M}_c c^2 \sim 2.8 \times 10^{35}$ ergs s^{-1}. The density of the stellar wind at the injection point of the jet is $n \sim 4 \times 10^{11}$ cm^{-2}, and the cross section for protons of $E_p \sim 1$ TeV is $\sigma_{pp} \sim 34$ mbarn. Hence, the mean free path of the protons is $\lambda_{pp} \sim 8.3 \times 10^{13}$ cm. The thickness of the region of the disk traversed by the jet is $\Delta z \sim r_{\rm perias} \tan 15^\circ \sim 4.4 \times 10^{11}$ cm. Consequently, we can approximate the gamma-ray luminosity by

$$L_\gamma = 2 f_\pi Q_j^{\rm rel}\left(1 - e^{-\Delta z/\lambda_{pp}}\right), \tag{7}$$

where $f_\pi \sim 0.2$ is the fraction of the energy of the leading proton that goes into neutral pions and hence into gamma rays. With a simple substitution into equation (7), we get $L_\gamma \sim 6.6 \times 10^{32}$ ergs s^{-1}, in good agreement with the detailed numerical calculations presented in Figure 3.

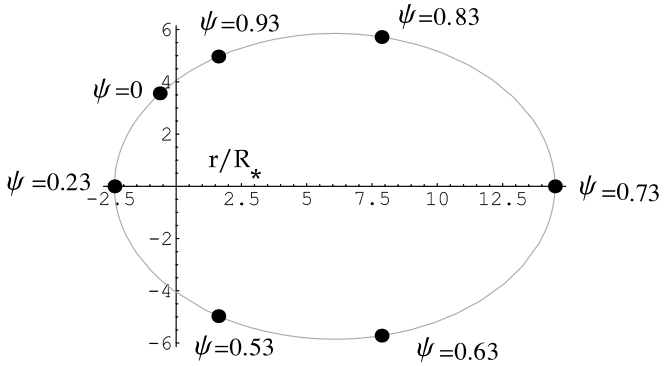

FIG. 2.—Orbit of LS I +61 303 drawn to scale, illustrating the geometry used in the calculations. The periastron passage occurs at 0.23 (Casares et al. 2005). [*See the electronic edition of the Journal for a color version of this figure.*]

4. OPACITY

The optical depth for a photon with energy E_γ, which in this case depends on the direction observed, can be estimated as

$$\tau(\rho, E_\gamma) = \int_{E_{\rm min}(E_\gamma)}^{\infty} \int_\rho^\infty n_{\rm ph}(E_{\rm ph}, \rho')\, \sigma_{e^-e^+}(E_{\rm ph}, E_\gamma)\, d\rho'\, dE_{\rm ph}, \tag{8}$$

where $E_{\rm ph}$ is the energy of the ambient photons, $n_{\rm ph}(E_{\rm ph}, \rho)$ is their density at a distance ρ from the neutron star, and $\sigma_{e^-e^+}(E_{\rm ph}, E_\gamma)$ is the photon-photon pair creation cross section given by

$$\sigma_{e^+e^-}(E_{\rm ph}, E_\gamma) = \frac{\pi r_0^2}{2}(1-\xi^2)\left[2\xi(\xi^2-2) + (3-\xi^4)\ln\left(\frac{1+\xi}{1-\xi}\right)\right], \tag{9}$$

where r_0 is the classical radius of the electron and

$$\xi = \left[1 - \frac{(m_e c^2)^2}{E_{\rm ph} E_\gamma}\right]^{1/2}. \tag{10}$$

In equation (8), $E_{\rm min}$ is the threshold energy for pair creation in the ambient photon field. This field can be considered to be formed by two components, one from the Be star and the other from the hot accreting matter impacting onto the neutron star: $n_{\rm ph} = n_{\rm ph,1} + n_{\rm ph,2}$. Here,

$$n_{\rm ph,1}(E_{\rm ph}, \rho) = \left[\frac{\pi B(E_{\rm ph})}{hcE_{\rm ph}}\right] \frac{R_*^2}{\rho^2 + r^2 - 2\rho r \sin\theta} \tag{11}$$

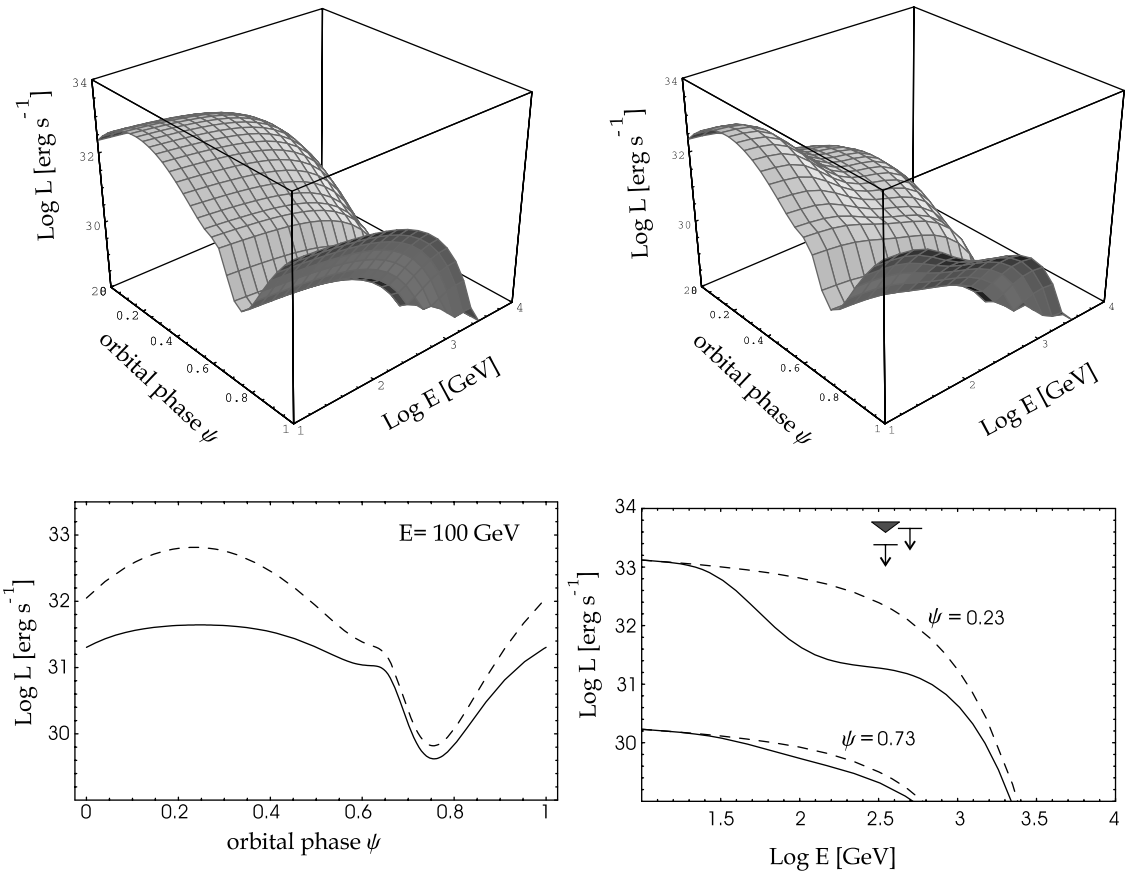

FIG. 3.—*Top left:* Three-dimensional plot of the generated luminosity as a function of the orbital phase and gamma-ray energy. *Top right:* Same plot, but taking into account the gamma-ray absorption in the ambient photon fields. *Bottom left:* Light curve for gamma rays of energy 100 GeV. The dashed curve corresponds to the generated luminosity, whereas the solid curve takes into account the effects of photospheric opacity. *Bottom right:* Spectral energy distribution at the periastron and apastron passage. The unabsorbed spectra are given by dashed lines. Upper limits from Whipple observations are indicated. [*See the electronic edition of the Journal for a color version of this figure.*]

is the blackbody emission from the star, with

$$B(E_{\rm ph}) = \frac{2E_{\rm ph}^3}{(hc)^2(e^{E_{\rm ph}/kT_{\rm eff}} - 1)} \qquad (12)$$

and $T_{\rm eff} = 22{,}500$ K (Martí & Paredes 1995). The separation r between the stars is again variable with the phase angle ψ.

The emission from the heated matter can be approximated by a bremsstrahlung spectrum,

$$n_{\rm ph,2}(E_{\rm ph}, \rho) = \frac{L_{\rm X}E_{\rm ph}^{-2}}{4\pi c\rho^2 e^{E_{\rm ph}/E_{\rm cutoff}}}, \quad \text{for } E_{\rm ph} \geq 1 \text{ keV}, \qquad (13)$$

where $L_{\rm X}$ is the total luminosity in hard X-rays and $E_{\rm cutoff} \sim 100$ keV. The photon index of the hard X-rays is taken to be within the range published by Greiner & Rau (2001), which was observationally determined. The luminosity $L_{\rm X}$ is also constrained by observations to be $L_{\rm X} \sim 10^{34}$ ergs s^{-1} (Paredes et al. 1997). Note that no bump due to a putative accretion disk has been observed at X-rays, so we neglect this contribution.

As an example, Figure 4 shows the dependence of the optical depth τ on the energy of the gamma rays and its variation along the z axis for the observer at $\theta_{\rm obs} = 30^\circ$. From detailed versions of this plot, we find that for photons of $E_\gamma = 100$ GeV, significant absorption occurs mostly between $\psi = 0.1$ and $\psi = 0.5$. The

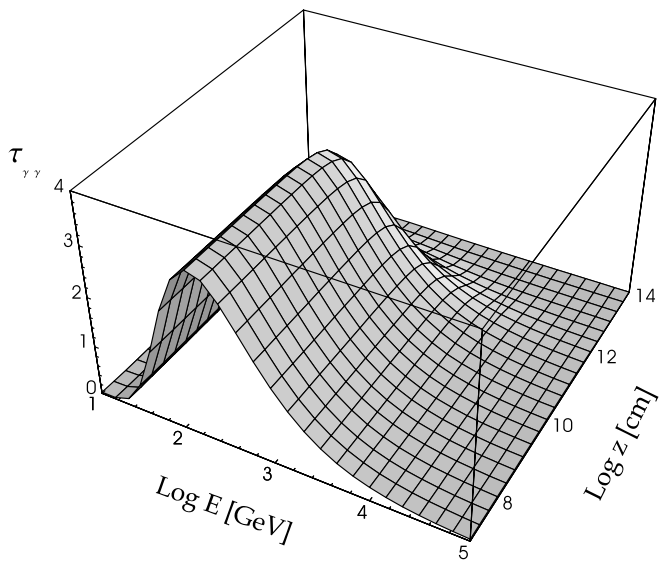

FIG. 4.—Opacity of the ambient photon fields to gamma-ray propagation. The figure corresponds to a viewing angle $\theta_{\rm obs} = 30^\circ$ and $\psi = 0.23$ (periastron). [*See the electronic edition of the Journal for a color version of this figure.*]

optical depth remains well below unity along the whole orbit for photons of energies $E_\gamma \lesssim 30$ GeV and $E_\gamma \gtrsim 2$ TeV.

5. SECONDARY ELECTRON-POSITRON PAIRS AND SYNCHROTRON EMISSION

Secondary pairs are produced by the decays of charged pions and muons, as well as by photon-photon interactions. The main reactions that lead to charged pions are

$$p + p \rightarrow p + p + \xi_{\pi^0}\pi^0 + \xi_{\pi^\pm}(\pi^+ + \pi^-), \quad (14)$$

$$p + p \rightarrow p + n + \pi^+ + X, \quad (15)$$

$$p + p \rightarrow 2n + 2\pi^+ + X, \quad (16)$$

where n is a neutron, X stands for anything (neutral) else, and the charged pion multiplicity is $\xi_{\pi^\pm} \approx 2(E_p/\mathrm{GeV})^{1/4}$. The neutrons have a proper lifetime of 886 ± 1 s, and since they move at ultrarelativistic speed, they can escape from the source, decaying at considerable distances (Eichler & Wiita 1978). On the other hand, pions decay into the jet trough $\pi^\pm \rightarrow \mu^\pm + \nu$ and $\mu^\pm \rightarrow e^\pm + \nu + \overline{\nu}$. For an injection proton spectrum given by equation (3) with $\alpha = 2.2$, we have that the pion spectrum (in the jet's system) will be a power law $J'_{\pi^\pm}(E'_{\pi^\pm}) = K_{\pi^\pm} E'^{-\alpha_\pi}_{\pi^\pm}$, with $\alpha_\pi \sim 2.3$. The electron-positron distribution mimics this power law (Ginzburg & Syrovatskii 1964; Dermer 1986):

$$J'_{e^\pm}(E'_{e^\pm}) = K_{\pi\rightarrow e^\pm} E'^{-\alpha_\pm}_{e^\pm}, \quad (17)$$

where

$$K_{\pi\rightarrow e^\pm} = \left(\frac{m_\mu}{m_e}\right)^{\alpha_\pm - 1} \frac{2(\alpha_\pm + 5)}{\alpha_\pm(\alpha_\pm + 2)(\alpha_\pm + 3)} K_{\pi^\pm} \quad (18)$$

and $\alpha_\pm = \alpha_\pi$.

The energy density of pion-generated pairs along the jet at the periastron passage can be calculated as

$$w_{\pi\rightarrow e^\pm} = \int (4\pi/c) E'_{e^\pm} J'_{e^\pm}(E'_{e^\pm})\, dE'_{e^\pm}, \quad (19)$$

where $J'_{e^\pm}(E'_{e^\pm})$ takes into account all the contributions from z_0 to $z_{\max}$. Integrating, we get $w_{\pi\rightarrow e^\pm} \approx 3 \times 10^9$ ergs cm^{-3}.

We can compare the energy density of pairs from the charged pion decays with that of the pairs produced by direct gamma-ray absorption. The total luminosity of these pairs is

$$L_{e^\pm} = L^0_\gamma (1 - e^{-\tau}). \quad (20)$$

Then, using the opacity calculated in § 4, the pair energy density is

$$w_{\gamma\gamma\rightarrow e^\pm} \sim \frac{L_{e^\pm}}{4\pi R_0^2 c}. \quad (21)$$

At the periastron passage, we get $w_{\gamma\gamma\rightarrow e^\pm} \approx 3.7 \times 10^9$ ergs cm^{-3}. Hence, the pair injection from the photon-photon annihilation is similar to that of pion decay. In what follows we evaluate the spectrum of these particles using the approximation derived by Aharonian et al. (1983), which is in excellent agreement with the more detailed calculations (exact to second order QED) presented by Böttcher & Schlickeiser (1997).

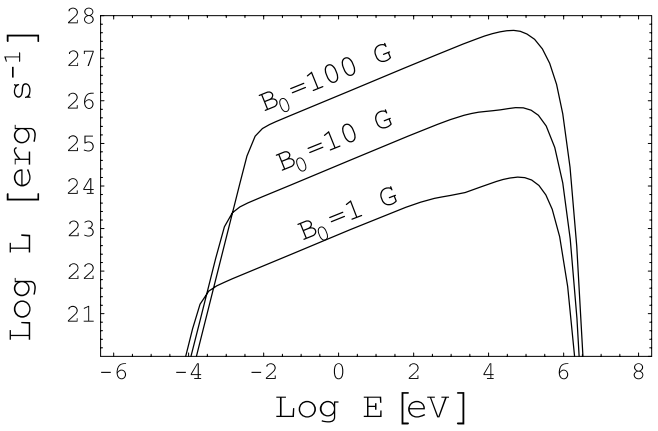

FIG. 5.—Synchrotron emission from secondary pairs.

The differential pair injection rate is given by (Böttcher & Schlickeiser 1997)

$$\dot{n}_{e^\pm}(\gamma) = \frac{3}{32} c\sigma_T \int_\gamma^\infty d\epsilon_\gamma \frac{N_\gamma(\epsilon_\gamma)}{\epsilon_\gamma^3} \int_{\epsilon_\gamma/[4\gamma(\epsilon_\gamma - \gamma)]}^\infty d\epsilon_{\mathrm{ph}} \frac{n_{\mathrm{ph}}(\epsilon_{\mathrm{ph}})}{\epsilon_{\mathrm{ph}}^2} \times \left\{ \frac{4\epsilon_\gamma^2}{\gamma(\epsilon_\gamma - \gamma)} \ln\left[\frac{4\epsilon_{\mathrm{ph}}\gamma(\epsilon_\gamma - \gamma)}{\epsilon_\gamma}\right] - 8\epsilon_\gamma\epsilon_{\mathrm{ph}} + \frac{2(2\epsilon_\gamma\epsilon_{\mathrm{ph}} - 1)\epsilon_\gamma^2}{\gamma(\epsilon_\gamma - \gamma)} - \left(1 - \frac{1}{\epsilon_\gamma\epsilon_{\mathrm{ph}}}\right) \frac{\epsilon_\gamma^4}{\gamma^2(\epsilon_\gamma - \gamma)^2} \right\}, \quad (22)$$

where $\gamma = E_{e^\pm}/m_e c^2$, $\epsilon_\gamma = E_\gamma/m_e c^2$, and $\epsilon_{\mathrm{ph}} = E_{\mathrm{ph}}/m_e c^2$. A numerical integration yields a pair spectrum that can be well fitted by a power law $N_{e^\pm} \propto E_{e^\pm}^{-1.9}$. The proportionality constant $K_{\gamma\gamma\rightarrow e^\pm}$ can be obtained from the absorbed gamma-ray luminosity.

The presence of a magnetic field in the jet implies that all these secondary pairs will produce synchrotron emission. Following Bosch-Ramon et al. (2005b), we assume that the magnetic field is entangled with cold protons in such a way that it has random directions, and hence the synchrotron emission is isotropic in the jet's frame. To calculate the synchrotron luminosity, we estimate the specific emission $[j_\epsilon(z)]$ and absorption $[k_\epsilon(z)]$ coefficients from the secondary particle distribution (see Pacholczyk 1970 for the detailed formulae) in such a way that

$$\frac{dL_\epsilon(z)}{dz} = 2\pi R_j \frac{j_\epsilon(z)}{k_\epsilon(z)} \left\{1 - \exp\left[-l_j k_\epsilon(z)\right]\right\}, \quad (23)$$

where to simplify the notation we are not using now primes to indicate that the calculation is in the jet's frame. In equation (23), $l_j \sim R_j$ is the typical size of the synchrotron emitting plasma, and ϵ is the photon energy in units of $m_e c^2$. Integrating over the jet length, we get the spectral energy distribution as

$$L^{\mathrm{obs}}_{\mathrm{syn}} = \epsilon \int_{z_0}^{z_{\max}} \delta^2 \frac{dL_\epsilon}{dz}\, dz, \quad (24)$$

where δ is the Doppler boosting factor defined as

$$\delta = \frac{1}{\Gamma(1 - \beta_b \cos\theta_{\mathrm{obs}})}. \quad (25)$$

To calculate the specific emission $j_\epsilon(z)$, we adopt different values of the magnetic field at z_0: $B_0 = 1$, 10, and 100 G (Bosch-Ramon &

Paredes 2004). In Figure 5 we show the spectral energy distribution of the synchrotron radiation of all secondary pairs for the three different values of B_0. The radio emission is quite negligible in comparison to the observed values, which at the minimum imply a luminosity of $\sim 10^{31}$ ergs s^{-1} (e.g., Ribó et al. 2005).

6. DISCUSSION

The predicted gamma-ray luminosity is clearly at its maximum during the periastron passage, when the neutron star travels through the densest parts of the wind. This is in accordance with the fact noticed by Massi (2004) that the peaks of the Energetic Gamma-Ray Experiment Telescope (EGRET) flux are coincident with the periastron and not with the radio maxima. The radio outbursts are the result of particle injection in the jet that occurs after some relaxation time from the periastron passage, when the accretion rate is increased (Paredes et al. 1991). Any purely leptonic model for the gamma-ray emission would have to explain why the radio and gamma-ray peaks are not observed in similar orbital phases.

Another specific feature of the gamma-ray emission predicted by our model is the presence of a local, secondary maximum at $\psi \sim 0.65$, when the accretion rate, given by equation (1), also has a local maximum due to the fact that the wind velocity is roughly parallel to the neutron star orbital velocity, hence reducing $v_{\rm rel}$ and increasing $\dot{M}_c$, as noticed by Martí & Paredes (1995).

The effects of the opacity of the ambient photon fields to gamma-ray propagation produces a "valley" in the spectral energy distribution, between a few tens of GeV and a few TeV, with a local minimum at around 100 GeV, during the periastron passage. The predicted luminosity is within the detection possibilities of an instrument like MAGIC, which, integrating over several periastron passages, could build up a spectral energy distribution that can be compared with that presented in Figure 3. Upper limits obtained with the Whipple telescope (Hall et al. 2003; Fegan et al. 2005) are indicated in the figure. The source is too weak for the sensitivity of this instrument according to our model.

7. CONCLUDING REMARKS

We have presented a hadronic model for the high-energy gamma-ray production in the microquasar LS I +61 303. The model is based on the interaction of a mildly relativistic jet with a small content of relativistic hadrons with the dense equatorial disk of the companion B0 V star. Gamma rays are the result of the decay of neutral pions produced by *pp* collisions. Charged pion decay will lead to neutrino production, which will be discussed elsewhere. The model takes into account the opacity of the ambient photon fields to the propagation of the gamma rays. The predictions include a peak of gamma-ray flux in the periastron passage, with a secondary maximum at phase $\psi \sim 0.65$. The spectral energy distribution presents a minimum around 100 GeV due to absorption. The spectral features should be detectable by an instrument like MAGIC through exposures $\sim$50 hr, integrated along different periastron passages.

We thank J. M. Paredes and V. Bosch-Ramon for careful readings of the manuscript and comments. The latter gave us useful support on calculations for the secondary emission. We also acknowledge constructive suggestions by an anonymous referee. This work has been supported by the Argentinian agencies CONICET and ANPCyT (PICT 03-13291). H. R. C. acknowledges support from FUNCAP and CNPq (Brazil).

REFERENCES

Aharonian, F. A., & Atoyan, A. M. 1996, A&A, 309, 917
Aharonian, F. A., Atoyan, A. M., & Nagapetyan, A. M. 1983, Astrophysics, 19, 187
Böttcher, M., & Schlickeiser, R. 1997, A&A, 325, 866
Bosch-Ramon, V., & Paredes, J. M. 2004, A&A, 425, 1069
Bosch-Ramon, V., Romero, G. E., & Paredes, J. M. 2005a, A&A, 429, 267
———. 2005b, A&A, submitted (astro-ph/0509086)
Casares, J., Ribas, I., Paredes, J. M., Martí, J., & Allende Prieto, C. 2005, MNRAS, 360, 1105
Dermer, C. D. 1986, ApJ, 307, 47
Eichler, D., & Wiita, P. J. 1978, Nature, 274, 38
Falcke, H., & Biermann, P. L. 1995, A&A, 293, 665
Fegan, S., et al. 2005, ApJ, 624, 638
Gaisser, T. K. 1990, Cosmic Rays and Particle Physics (Cambridge: Cambridge Univ. Press)
Ghisellini, G., Maraschi, L., & Treves, A. 1985, A&A, 146, 204
Ginzburg, V. L., & Syrovatskii, S. I. 1964, Soviet Astron., 8, 342
Gregory, P. C. 2002, ApJ, 575, 427
Gregory, P. C., & Neish, C. 2002, ApJ, 580, 1133
Gregory, P. C., & Taylor, A. R. 1978, Nature, 272, 704
Greiner, J., & Rau, A. 2001, A&A, 375, 145
Hall, T. A., et al. 2003, ApJ, 583, 853
Kaufman Bernadó, M. M., Romero, G. E., & Mirabel, I. F. 2002, A&A, 385, L10
Kniffen, D. A., et al. 1997, ApJ, 486, 126
Kotani, T., Kawai, N., Matsuoka, M., & Brinkmann, W. 1996, PASJ, 48, 619
Kotani, T., et al. 1994, PASJ, 46, L147
Martí, J., & Paredes, J. M. 1995, A&A, 298, 151
Massi, M. 2004, A&A, 422, 267
Massi, M., Ribó, M., Paredes, J. M., Garrington, S. T., Peracaula, M., & Martí, J. 2004, A&A, 414, L1
Massi, M., Ribó, M., Paredes, J. M., Peracaula, M., & Estalella, R. 2001, A&A, 376, 217
Migliari, S., Fender, R., & Méndez, M. 2002, Science, 297, 1673
Pacholczyk, A. G. 1970, Radio Astrophysics (San Francisco: Freeman)
Paredes, J. M., Martí, J., Estalella, R., & Sarrate, J. 1991, A&A, 248, 124
Paredes, J. M., Martí, J., Peracaula, M, & Ribó, M. 1997, A&A, 320, L25
Paredes, J. M., Martí, J., Ribó, M., & Massi, M. 2000, Science, 288, 2340
Purmohammad, D., & Samimi, J. 2001, A&A, 371, 61
Ribó, M., Combi, J. A., & Mirabel, I. F. 2005, Ap&SS, 297, 143
Romero, G. E., & Orellana, M. 2005, A&A, 439, 237
Romero, G. E., Torres, D. F., Kaufman Bernadó, M. M., & Mirabel, I. F. 2003, A&A, 410, L1
Tavani, M., Kniffen, D. A., Mattox, J. R., Paredes, J. M., & Foster, R. 1998, ApJ, 497, L89